Characterizing Foam Flow in Fractures for Enhanced Oil Recovery

Alquaimi, Bander; Rossen, Bill

DOI
10.3997/2214-4609.201700336

Publication date
2017

Document Version
Accepted author manuscript

Published in
IOR NORWAY 2017

This is an Accepted Manuscript of a paper published by EAGE
IOR NORWAY 2017: Proceedings of 19th European Symposium on Improved Oil Recovery,
24-27 April 2017, Stavanger, Norway
https://doi.org/10.3997/2214-4609.201700336

Characterizing Foam Flow in Fractures for Enhanced Oil Recovery

B. I. AlQuaimi, W. R. Rossen
Department of Geoscience and Engineering, Delft University of Technology

Abstract

Gas is very efficient in displacing oil for enhanced-oil-recovery projects because of its high microscopic-displacement efficiency. However, the process at the reservoir scale suffers from poor sweep efficiency due to density and viscosity differences compared to in-situ fluids. Foam substantially reduces the viscosity of injected gas and hence improves the sweep. Foam rheology in 3D geological porous media has been characterized both theoretically and experimentally. In contrast, the knowledge of foam flow in fractured porous media is far less complete.

We study foam rheology in a fully characterized model fracture. This investigation is conducted by varying superficial velocities of gas and surfactant solution. We find in this model fracture the same two foam-flow regimes central to the understanding of foam in 3D porous media: a low-quality regime where pressure gradient is independent of liquid velocity and a high-quality regime where pressure gradient is independent of gas velocity. The transition between regimes is less abrupt than in 3D porous media. Direct observation of bubble size, bubble trapping and mobilization, and foam stability as functions of superficial velocities allows comparison with our understanding of the mechanisms behind the two flow regimes in 3D porous media. Additionally, foam is shear-thinning in both regimes. But in other important respects the mechanisms thought to be behind the two flow regimes in 3D media do not appear in our model fracture. Foam is not at the limit of stability in the high-quality regime. Mobility in the high-quality regime instead reflects reduced and fluctuating foam generation at high foam quality.

Introduction

Underground reservoirs that include natural fractures impose additional challenges for enhanced-oil-recovery (EOR) projects. The challenges are encountered because of the presence of highly conductive fractures or fissures (Allan & Sun, 2003). Injected fluids designed to recover un-displaced oil flow rapidly in the fractures, reducing the efficiency of the process. Foam greatly reduces gas mobility and hence allows gas to encounter more oil (Fjelde et al., 2008; Haugen et al., 2014; Steinsbø et al., 2015). Numerous studies have characterized foam rheology in 3D geological porous media, both theoretically and experimentally, but far fewer for fractured porous media.

Kovscek et al. (1995) investigated nitrogen, water and aqueous foam flow through two transparent replicas of natural rough-walled rock fractures with hydraulic apertures of both roughly 30 μm and 100 μm. Radial-flow tests were done on these fractures, with a diameter of 12 cm. The total flow rate of nitrogen ranged from 1-100 SCCM, which is equivalent to 0.0014-0.147 m/s. They concluded that the rheology of foam in fractures is complicated. At gas fractional flows, i.e. foam qualities, above 0.97 the pressure drop was proportional to the

liquid flow rate at a fixed gas flow rate. For gas fractional flows below roughly 0.9, the pressure drop was insensitive to liquid flow rate. At intermediate gas fractional flow, the pressure drop decreased with increasing liquid flow rate.

Buchgraber et al. (2012) experimentally investigated the behaviour of pre-generated foam in fractures at various foam qualities and fluid velocities. The experiments were conducted in fractures etched on 2X5 cm silicon chips. The first experiment was done in smooth channels with apertures of 40 and 30 μm. The second experiment was conducted on a smooth slit with apertures of 20 and 40 μm arranged in a checkerboard pattern. The third experiment involved a fracture with a rough face. The gas superficial velocity ranged from 0.0 - 0.0057 m/s and the liquid superficial velocity ranged from 0.0 – 0.0017 m/s. Low- and high-quality regimes were identified. They explain the low pressure gradient observed in the high quality regime as the result of coalescence of foam.

Fernø et al. (2016) reported a study of foam flow behaviour in a fractured rock slab 31.2 cm long. The total superficial velocities used were 0.0003, 0.001, 0.0017 and 0.0028 m/s. Increased pressure gradient was observed at increased foam quality, for a given total flow rate. At high foam quality the pressure gradient suddenly dropped. They explain this sudden decrease as the result of the dry conditions leading to foam coalescence.

In this study, we investigate the rheology of in-situ generated foam in a well-characterized transparent model fracture. We compare the behaviour of foam using four total superficial velocities (0.0011, 0.0021, 0.0030, and 0.0049 m/s) and foam qualities ranging from 23 to 97%. We measure the pressure difference across four sections along the fracture and capture images to explain foam behaviour.

Fracture Physical Model

This fracture apparatus and the model fracture were used previously to study foam generation and propagation in fractures (AlQuaimi & Rossen, 2017b). The 40 X 10 cm model fracture consists of a roughened plate that represents fracture wall roughness and a top plate that is smooth, to allow direct observation of the flow. The 4-mm-thick roughened plate was strengthened by attaching a 15-mm-thick glass plate using ultraviolet light and DELO®-Photobond® glue (DELO, Windach, Germany). The thickness of the top glass plate is 15 mm as well. The thickness of the glass was estimated based on solid-mechanics calculations to prevent any glass deflection during the flow. This is also checked using a digital-feeler meter (2μ resolution) during the experiment. The roughened plate include two inlet ports that allow separate co-injection of gas and liquid. The inlet ports are connected to a 8.0X2.0X0.04 cm entry region milled in the roughened plate for the gas and liquid to collect before they enter fracture. Four pressure ports are equally spaced over a length of 36 cm and fluid outlet. The gap between the top plate and the rough surface represents the fracture aperture. The two glass plates are glued together using Araldite® 2014, which is a two-component epoxy adhesive that has a tensile strength of 26 Mpa at 23°C. The fracture is mounted in a frame that could slide 50 cm in the X and Y directions to allow for microscopic observation of flow in the whole 40X10 cm fracture.

The model fracture has been characterized in terms of average aperture and variability and correlation length of aperture, allowing its representation as a 2D porous medium with pore throats and bodies. Using this characterization we previously combined the capillary number-residual saturation curve for a wide range of model fractures into a single relationship

(AlQuaimi & Rossen, 2017a). This study is part of a larger effort to examine foam behaviour in a wide variety of model fractures and relate the behaviour to dimensionless correlations that can be applied to natural fractures of all types in the field.

Fracture Characterization

This model fracture has a regular pattern in its roughness. The roughened glass sample was profiled using NPFLEX^{TM} White Light Interferometer Optical Profiling (Philips Innovation Services, Eindhoven, The Netherlands), to quantify the spatial and vertical variations in height. The sample to be profiled was coated by depositing a layer of silver 150 nm thick to enhance the reflection. Since it is a regular pattern of roughness the measurement was performed on 1.0x1.0 cm patch of the glass, with lateral resolution of 3.6 µm (Fig 1).

A fracture can be considered as a two-dimensional network of pore bodies (maxima in aperture) connected by throats (saddle points between pore bodies). Several methods are available in the literature to extract a realistic pore network for rock samples (Rabbani et al., 2014). The method we use is based on a simple concept using flood-fill and image-slicing (AlQuaimi & Rossen, 2017a). A MatLab® (The MathWorks Inc., Eindhoven, The Netherlands) code was developed to highlight all areas with height less than some threshold and then produce images at every 5 µm increments in height. An isolated, deep region represents a pore body. When two regions join upon increasing height, the connection between them is a pore throat. The sequence of images are loaded into ImageJ, an open-source Java image-processing program, to identify the pore throats and draw the pore-body boundaries. Characteristic pore-throat aperture (d_t) is taken at the percolation threshold, pore-body aperture (d_b) is the average pore-body aperture, and pore-length (L_p) is the average pore body length of the 2D network in the flow direction (Figs 2 and 3). The hydraulic aperture is determined experimentally by injecting water and obtaining the flow rate-pressure drop relationship.

Table 1 summarizes the fracture aperture data. The table also shows the characteristics of the rough surface. Additional details on the characterization of the fracture data are reported by AlQuaimi and Rossen (2017a).

Table 1 Fracture Aperture and roughness data (all in µm)

Pore-throat aperture, d_t	60
Pore-body aperture, d_b	130
Hydraulic aperture (experimentally determined), d_H	66
Pore Length, L_p	815
Arithmetic average absolute deviation from average height, S_a	29.10
Root-Mean-Square deviation from average height , S_q	33.70

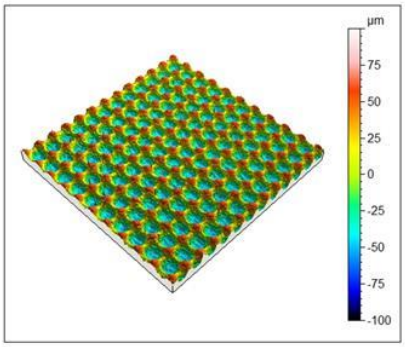

Figure 1. *Bottom glass surface topography*

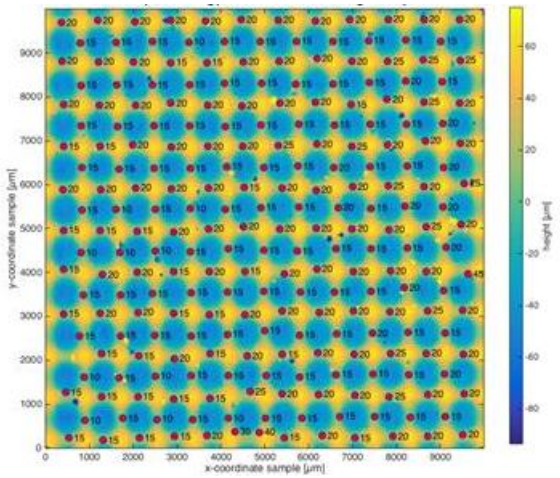

Figure 2. *Pore-throat locations*

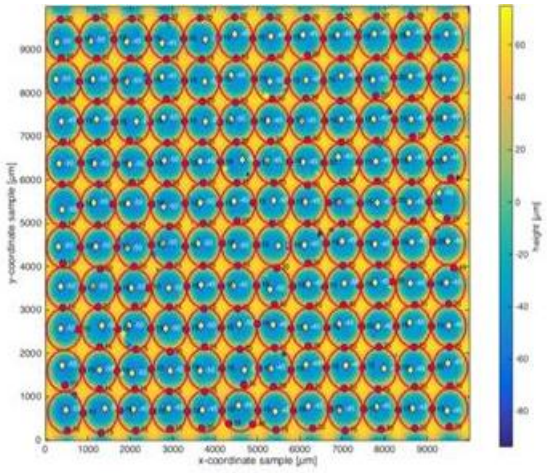

Figure 3. *2D Network of pore body and pore throat*

Experimental Setup

The model fracture discussed above is the centrepiece of the setup. Sodium C14-16 olefin sulfonate (Bio-Terge®- AS-40 KSB, Stepan, Voreppe, France), an anionic surfactant with 39 wt. % active component and a critical micelle concentration (cmc) of 301.0 mg/l, was used to generate foams. A 1.0 wt.% surfactant solution was used in all experiments. The surfactant solution is injected using a Standard Infusion PHD Ultra Syringe Pump (Model-703005, Harvard Apparatus, Holliston, USA). Flow rates are stated to be accurate within 0.25%, with reproducibility within 0.05% of full scale. This pump is equipped with micro-stepping techniques to further reduce flow pulsation. The pump has a range from 0.0001 µl/hr to 216 ml/min. There is no imposed back-pressure on the apparatus.

The nitrogen is injected through a gas mass-flow meter/mass-flow controller (EL-Flow® F-230M-RAD-22-K, Bronkhorst High-Tech B.V., Ruurlo, Netherlands) which has a range of 0-10 mln/min. The bottom glass plate consists of three pressure ports with a distance of 9.0 cm between them to provide pressure readings across the whole surface. The pressure-difference sensors (MPXV5050DP, Freescale Semiconductor, Inc., Austin, TX, USA) are integrated silicon-on-chip, signal-conditioned and temperature-compensated. They have a range from 0 to 50 kPa (0 to 7.25 psi) with a maximum error of 5.0% from 0°C to 85°C. The sensors are connected to a data-acquisition unit and a computer, where pressures are recorded every second.

For monitoring foam flow a LEICA MZ 8 Microscope (10445538 1.0X, Leica Microsystems B.V., Amsterdam, Netherlands) was used. The Microscope is connected to DRS's LIGHTNING RDTTM camera, consisting of a small camera head, detachable cable and custom frame-grabber board. The Lightning RDTTM is ultrafast and high-resolution and captures 1,280 x 1,024-resolution images at 500 full frames per second (fps). Higher fps of 16,000 can be achieved at reduced resolution for recording extremely rapid events. MiDAS 2.0 (Xcitex Inc., Woburn, USA) camera-control software was also used to process the images/videos in real time during recording.

A compact backlight (model CVI STAR-BL-110/110-WH-24V; Stemmer® Imaging B.V., Zutphen, Netherlands) provides constant and even illumination. Uniform light is needed to produce noise-free images which are used to monitor foam flow. Figs. 4 and 5 show the experimental setup.

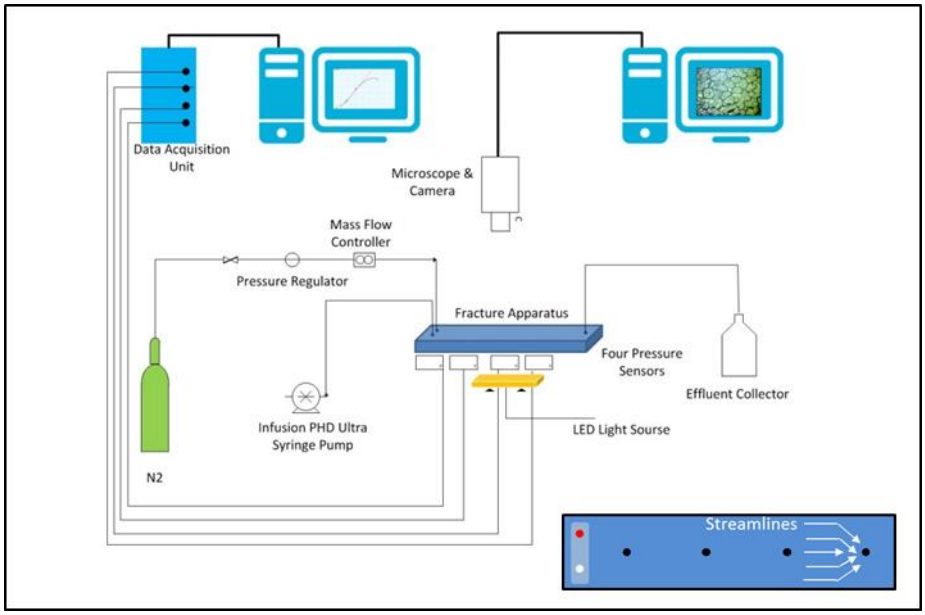

Figure 4. *Schematic of experimental setup*

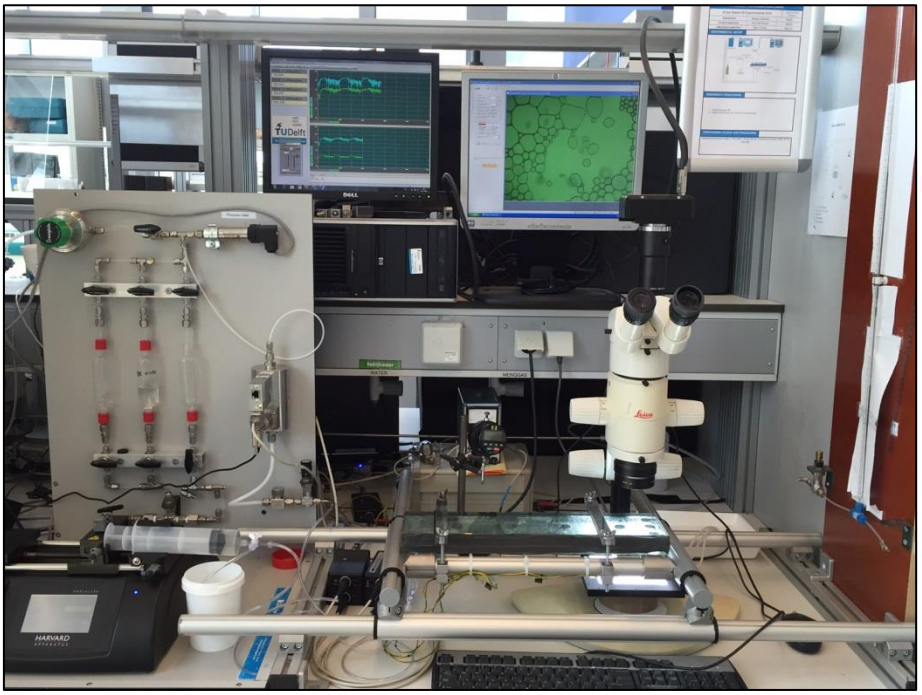

Figure 5. *Photo of experimental setup*

Experimental Procedure

We vacuum the model fracture and inject demineralized water to displace all the air from the system. We next measure the hydraulic aperture of the model fracture by incrementally increasing water injection rate and recording pressure. The rate-pressure relationship was used to estimate the hydraulic aperture (Chen et al., 2004; Fernø et al., 2016; Hakami & Larsson, 1996; Witherspoon et al., 1980):

$$Q = \frac{1}{12}\frac{|\nabla P| w d_H^{\,3}}{\mu} \tag{1}$$

where Q is volumetric flow rate, $|\nabla P|$ is pressure gradient, w is the width, d_H is the hydraulic aperture, and μ is the viscosity. The flow experiments for our model fractures showed a linear relationship between Q and $|\nabla P|$, which indicates that the inertial forces were negligible and there was no change in aperture during flow (Fig. 6).

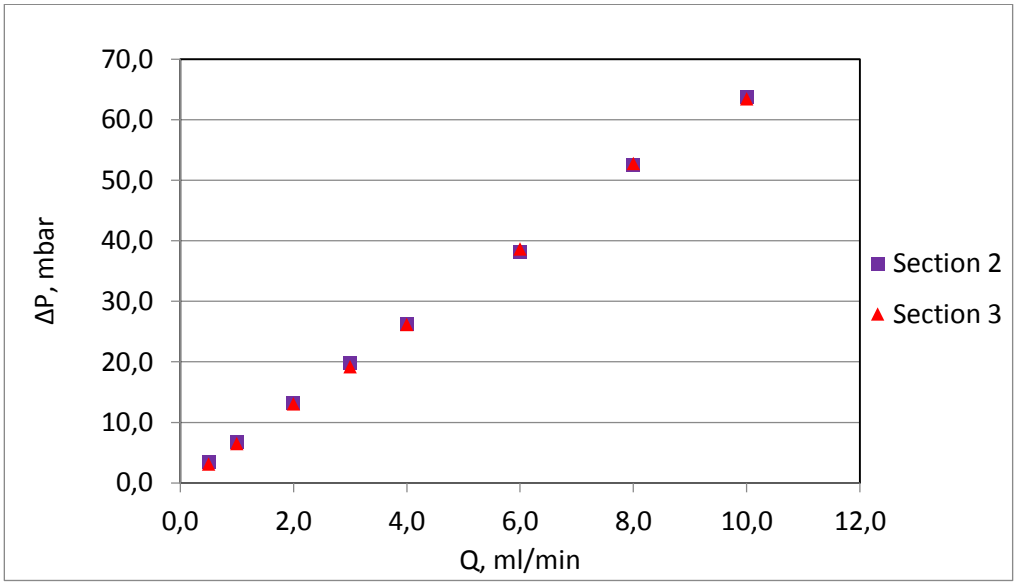

Figure 6. *Rate-Pressure drop relationship*

The pressure gradient in the first section is affected by the entry region and the last one by converging flow towards the outlet, so they were not used in the analysis (Fig. 4). The hydraulic aperture of this model fracture is 66 µm.

The foam experiment starts by co-injecting a solution of 1.0 wt.% sodium C14-16 olefin sulfonate and nitrogen into the fully water-saturated fracture. The two fluids enter the model fracture at the entry region and flow into the fracture. In-situ foam generation is observed as discussed in our first report (AlQuaimi & Rossen, 2017b). Pressure gradient is recorded until stabilization is reached (Fig. 7). The figure shows the evolution of pressure gradient as the water initially present is displaced and foam is generated. The test was conducted at a foam quality (f_g) of 37% and total superficial velocity of 0.0021 m/s. Oscillation is observed in this test and larger oscillation is evident at high f_g. In 3D porous media similar behavoir would be

due to rapid generation and destruction at high f_g (Prigiobbe et al., 2016; Ransohoff & Radke, 1988). We selected the third section on which to base our analysis of the pressure behavoir in this paper. We averaged the pressure gradient over period of stabilization for each foam quality. The injected gas volume is corrected to the pressure at the middle of the fracture. We performed foam-quality scans at fixed total superficial velocity (u_t). The pressure-gradient data are acquired in a random sequence to avoid any hysteresis that may occur in case of sequential increase or decrease in f_g (Fig. 8). The data points have symbols which indicate the sequence in which they were acquired. The error bars in the plot indicate the standard deviation of the measurement. Additionally, point 3 at $f_g = 0.25$ was repeated after displacing all the foam and starting the experiment again with only water in the fracture. This gives extra confidence in the measurement and the procedure followed to acquire the data. The oscillation in $|\nabla P|$ reflects fluctuation in foam generation, as discussed below.

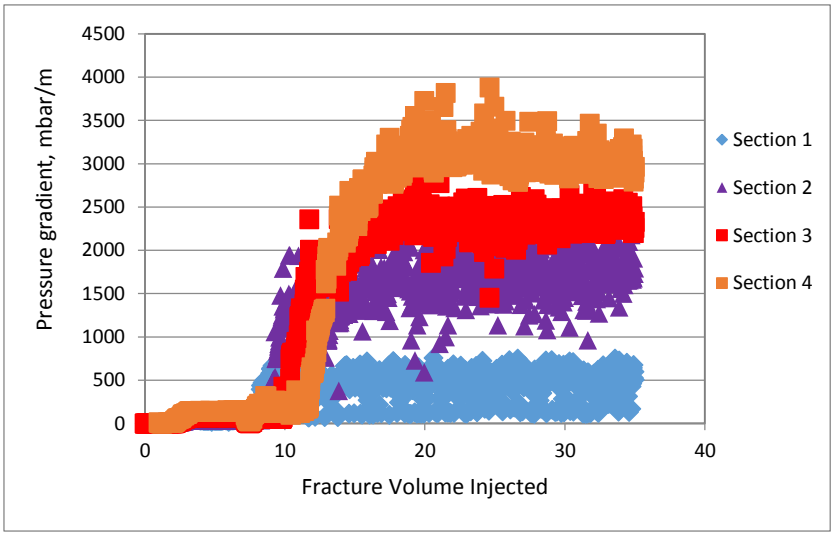

Figure 7. *Pressure gradient of foam injection test at foam quality of 37%*

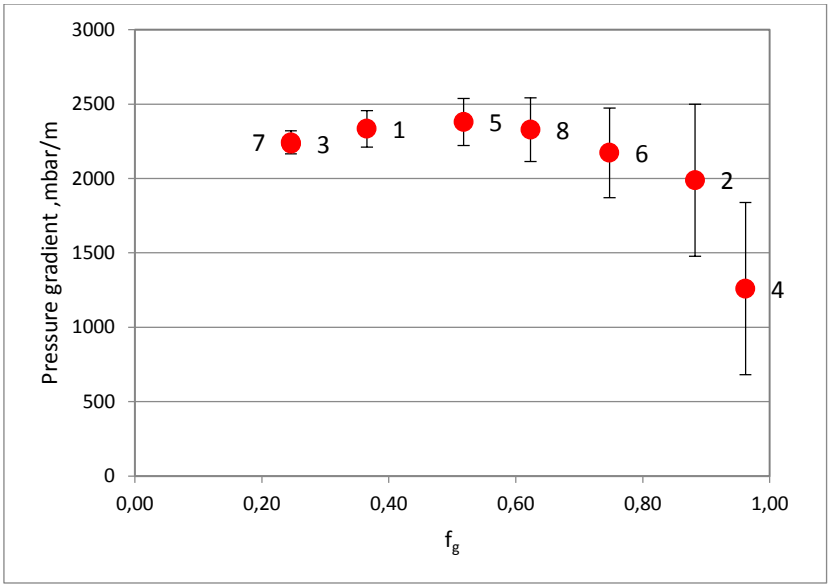

Figure 8. *Foam quality scan at u_t = 0.0021 m/s*

Experimental results

We tested four total superficial velocities u_t, after confirming the validity of the test procedure. The tested velocities are 0.0010, 0.0021, 0.0030, and 0.0049 m/s (Fig. 9). As the velocity increases the pressure gradient increases; however, the increase is not proportional to u_t. The 42% increase in u_t from 0.0021 to 0.0030 m/s gives little increase in pressure gradient. At total superficial velocity of 0.0010 m/s, the lowest f_g that can be achieved with our gas mass-flow meter/mass-flow controller is 0.38. We used Eq. (1) to estimate foam apparent viscosity in these four tests (Fig. 10). The largest mobility reduction is achieved in these tests at velocity of 0.0010 m/s. A mobility reduction by a factor of 67 relative to that of water in single-phase flow is estimated at f_g of 0.53. If we estimate mobility reduction to gas, this estimate would be several orders of magnitude. Fig. 10 indicates that foam is shear-thinning and Fig. 11 shows that foam apparent viscosity is shear-thinning with respect to superficial velocity with average exponent of about (-0.82).

Figure 9. *Foam quality scan at different total-injection velocities(m/s).*

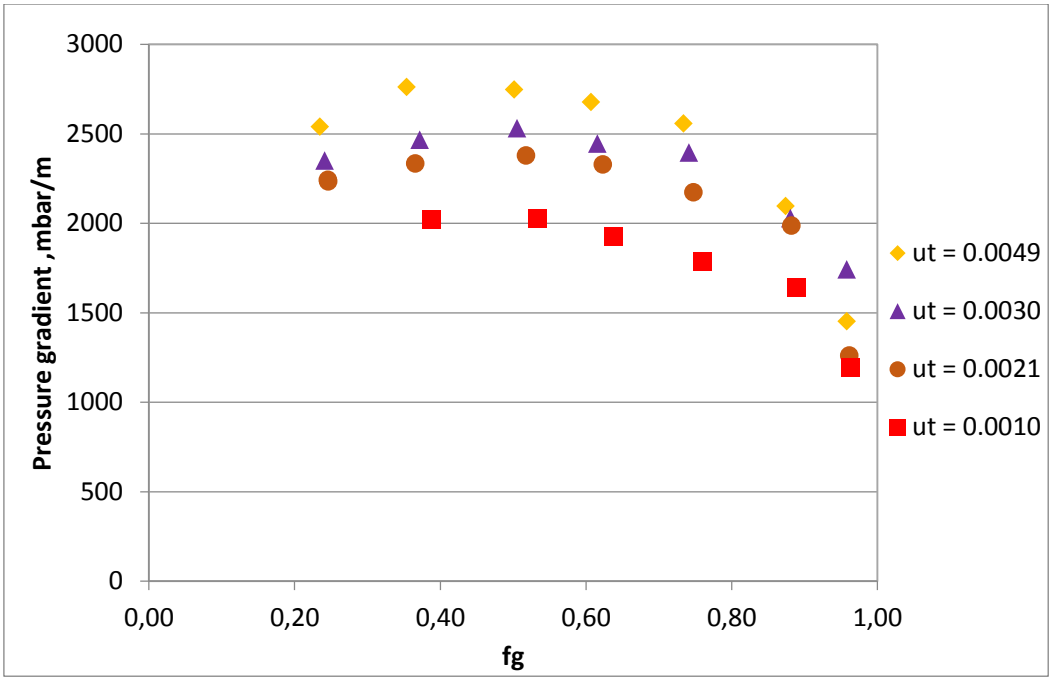

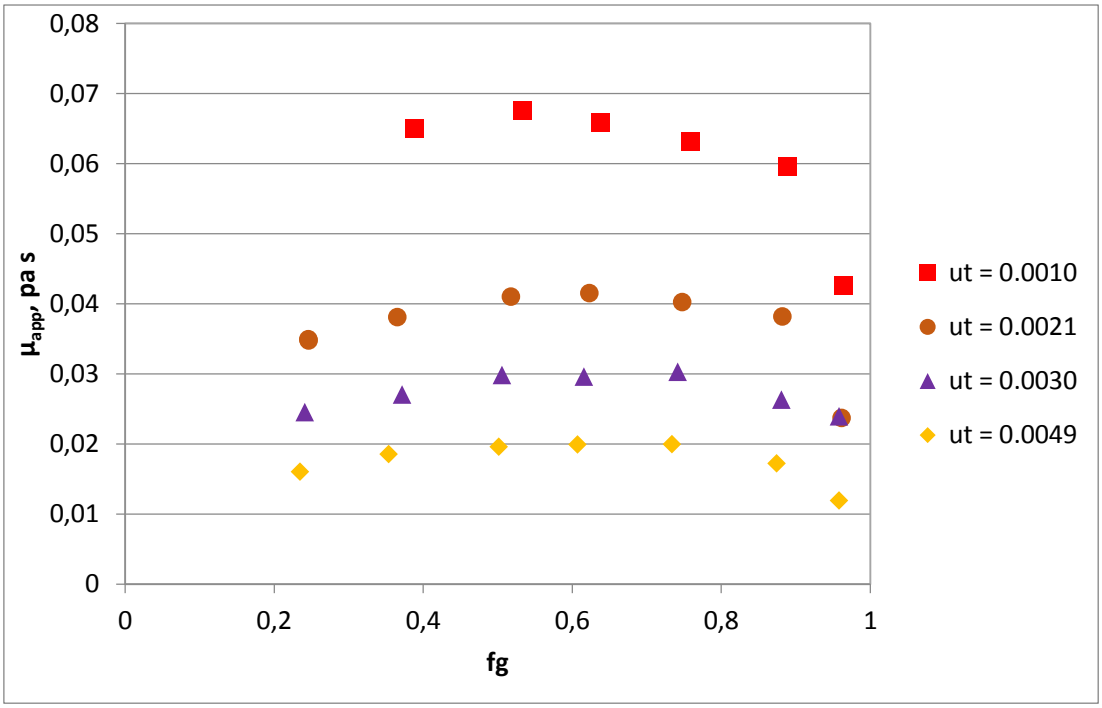

Figure 10. *Foam apparent viscosity at different total-injection velocities*

Figure 11. *Foam viscosity shear-thinning behaviour*

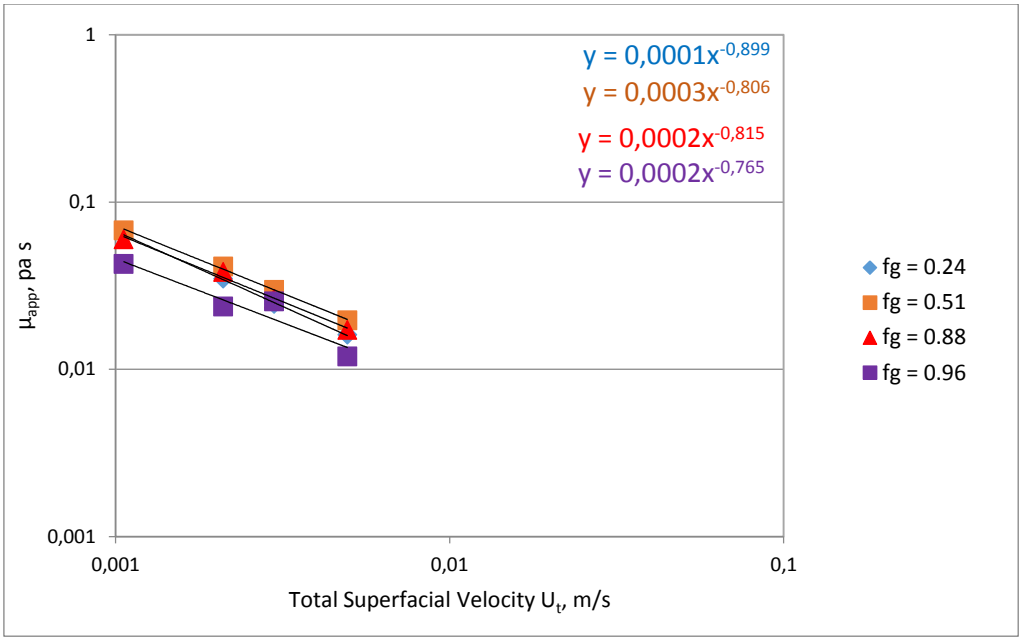

Central to the understanding of flow in 3D porous media is the existence of two distinct foam-flow regimes, corresponding to high foam quality and low foam quality (Alvarez et al., 2001). Pressure gradient is independent of liquid velocity in the low-quality regime and independent of gas velocity in the high-quality regime. We investigated the existence of these two flow regimes in our model fracture. The pressure-gradient data were plotted using a Julia (open source programming language) script, which is written to construct a contour plot from the data. The plot shows the existence of two flow regimes in the fracture similar to those in 3D porous media (Fig. 12). Fig. 12 reveals a broader transition between the two qualities than usually seen in 3D porous media. The explanation for pressure-gradient behaviour in the high-quality regime in 3D porous media is that foam collapse at the limiting capillary pressure (P_C*) controls bubble size and therefore gas mobility (Khatib et al., 1988). In the low-quality regime, bubble size thought to be unchanging and pressure gradient depends on porous medium and to lesser extent on surface tension, but not on ability of surfactant to stabilize foam (Rossen & Wang 1999). The transition between regimes is sensitive to both the nature of the porous medium and ability of surfactant to stabilize foam (Alvarez et al., 2001).

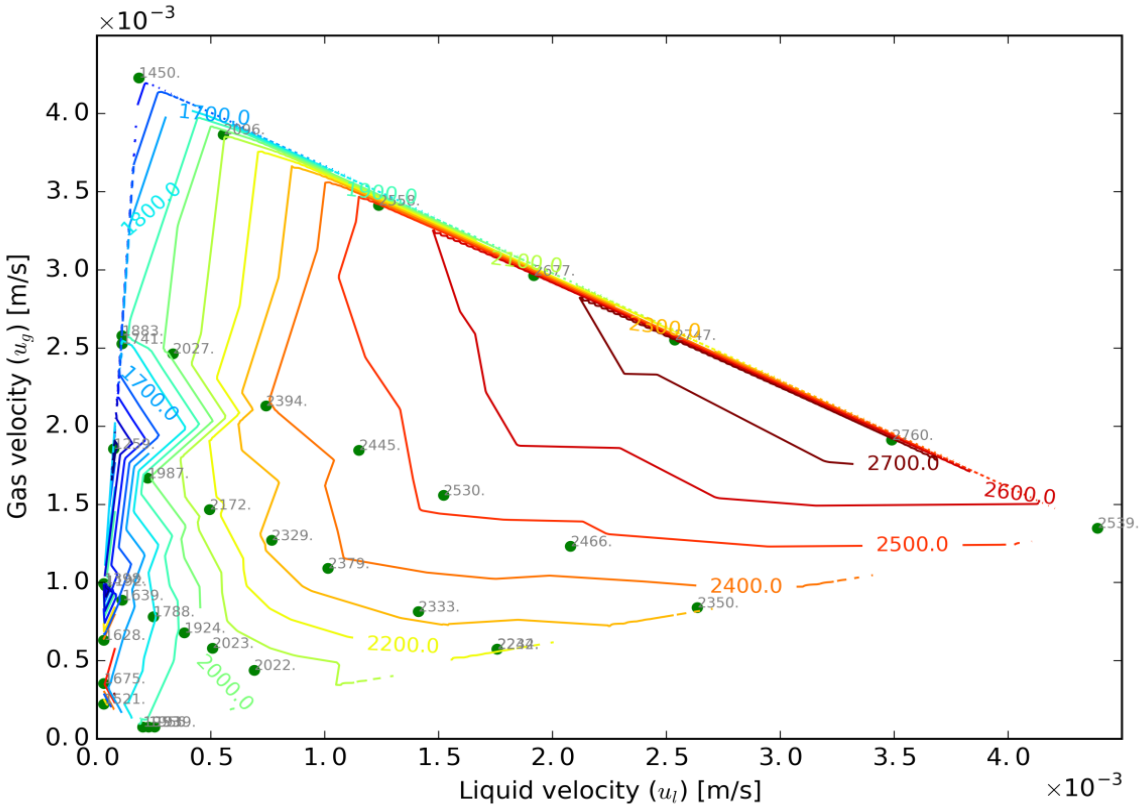

Figure 12. *Existence of two f low regimes in fracture*

In our model fracture, we observe different phenomena that contribute to the existence of the two flow regimes. Several images were captured and analysed using ImageJ, which is an image-processing and analysis software. We developed a procedure for the analysis of the images using image-thresholding to detect the boundary of the foam bubbles and determine bubble sizes. At high foam quality, we see reduced and fluctuated foam generation and steady foam generation at low quality. At high foam quality, fine-textured foam is generated and propagates, followed by a slug of gas that is refined as it propagates (Fig. 13). This causes the pressure response to fluctuate and hence reduces time-average foam apparent viscosity. Fig. 13 also shows the time interval between the individual gas slugs at u_t of 0.0030 m/s and f_g of 0.90. The length of the gas slug and its velocity increase as f_g increases (Fig. 14). Fig. 14 shows that the time interval between the gas slugs is much shorter and the size of the gas slugs is much larger than in the previous case, such that a micro image would be completely occupied by the slug. At low foam quality, foam is generated mainly by capillary snap-off and the average bubble size remains constant at a size less than pore size (Fig. 15).

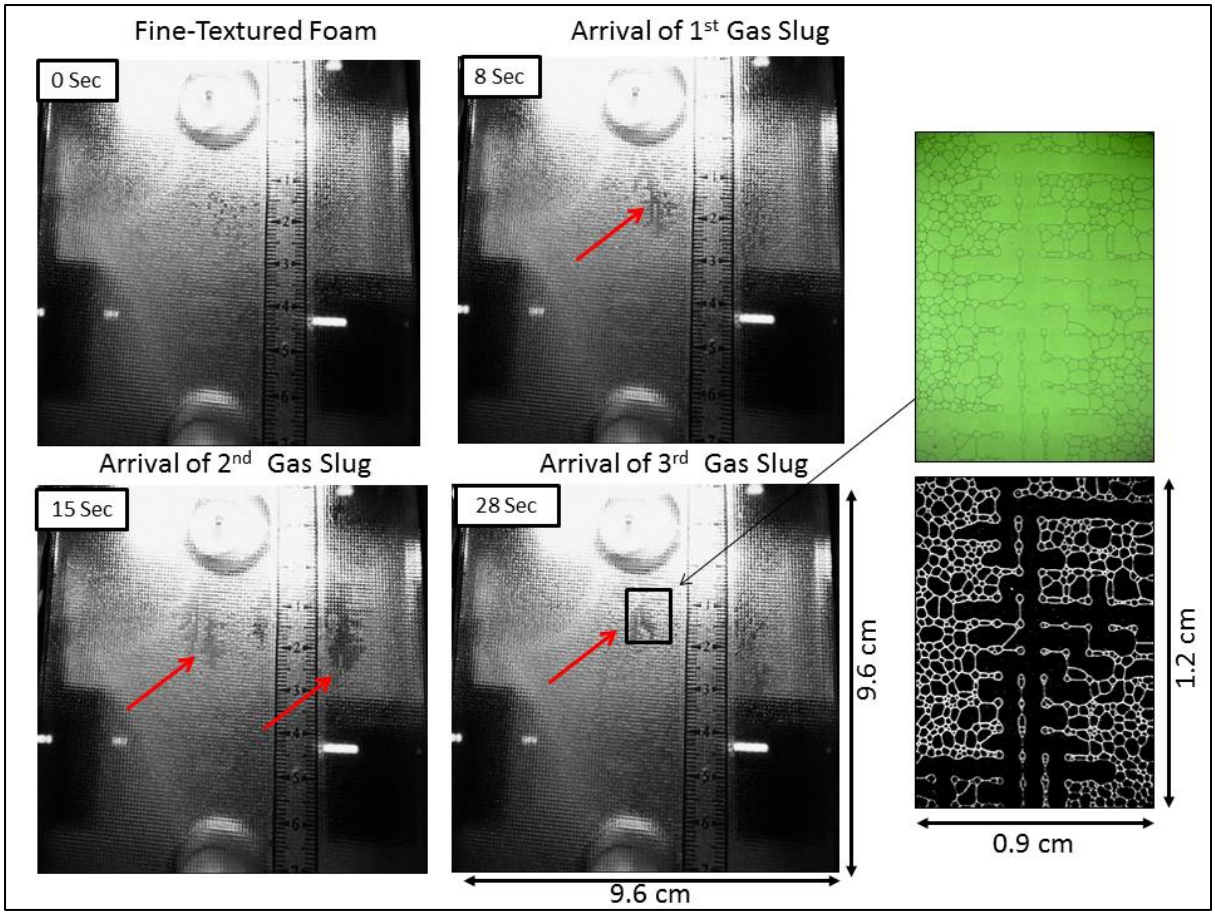

Figure 13. *Time-lapse images of reduced and fluctuating foam generation. The micro images at right show the gas slug. (This binary image is the processed version: black is gas and white is foam films (lamellae.) Total superficial velocity* u_t *= 0.0030 m/s and* f_g *= 0.90.Flow is from the top of the image to the bottom.*

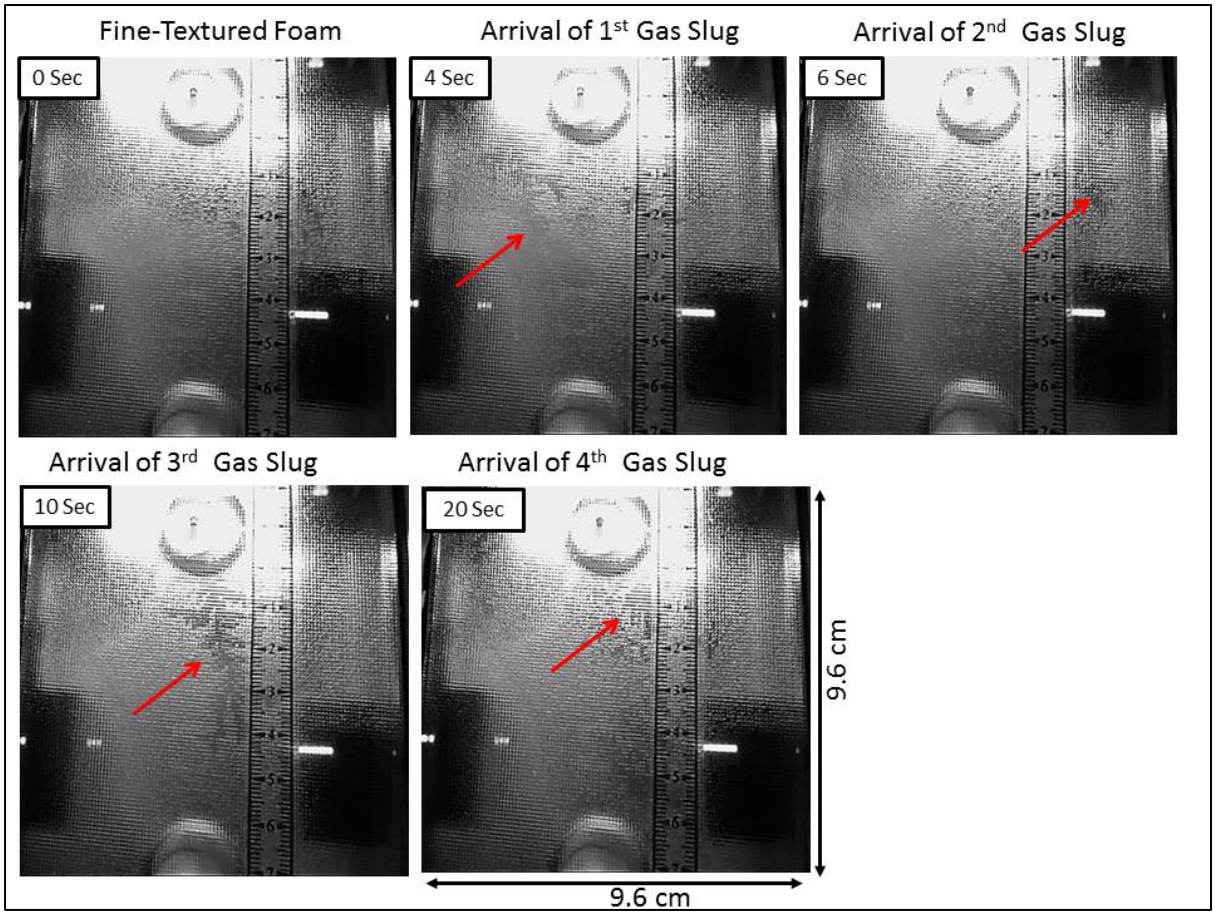

Figure 14. *Time-lapse images show reduced and fluctuating foam generation. Total superficial velocity u_t = 0.0030 m/s and f_g = 0.96. Flow is from the top of the image to the bottom.*

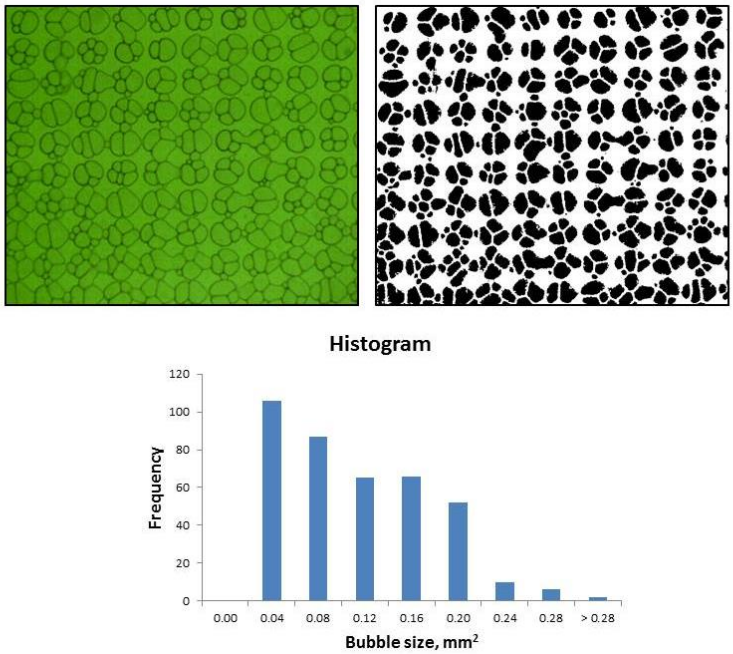

Figure 15 *0.97X0.82 cm image and the binary version of it. Black is gas and white is water. The histogram shows the bubble-size distribution. Foam was generated at u_t = 0.0010 m/s and f_g = 0.38.*

Three low values of f_g, 0.24, 0.38 and 0.51, are used to investigate the foam texture at different u_t. The pressure gradient, as shown in Fig. 9, increases as u_t increases at a fixed f_g. However, we find for the these values of u_t the average bubble size does not change greatly at fixed f_g (Figs. 16, 17, and 18). It is thought that average bubble size is unchanging in the low-quality foam regime in 3D porous media (Alvarez et al., 2001; Rossen & Wang 1999). Bubbles are thought to be as large as pores in that regime. The near-invariance of bubble size in Figs. 16 to 18 is consistent with these findings, but bubbles are smaller than pores. The error bar on the average bubble size represents the standard deviation of bubble-size distribution.

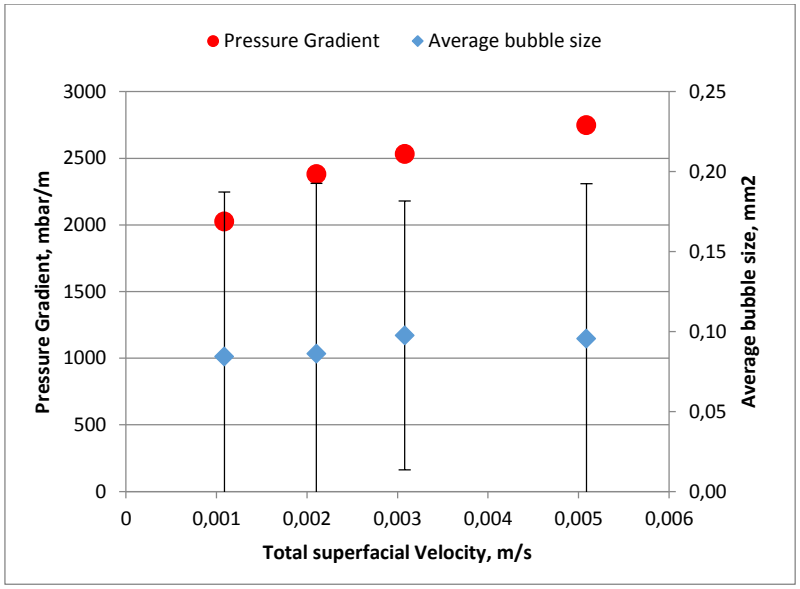

Figure 16. *Pressure gradient and average bubble size vs u_t at f_g = 0.51.*

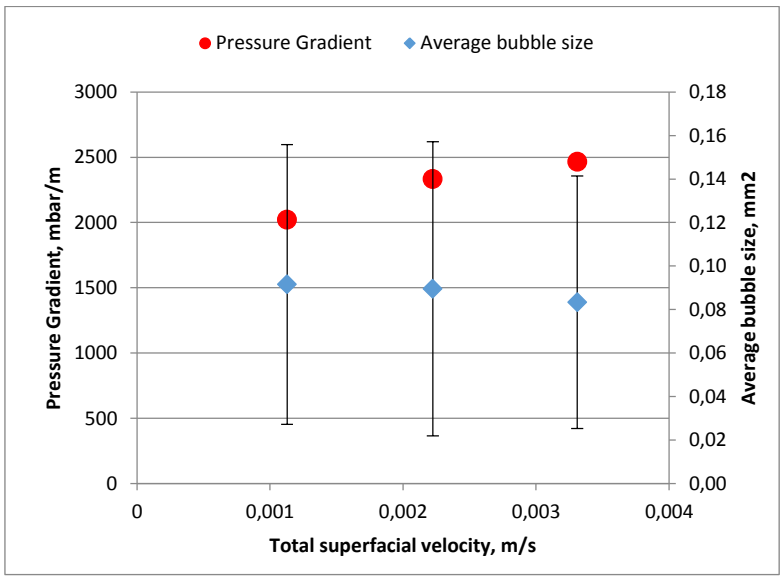

Figure 17. *Pressure gradient and average bubble size vs u_t at f_g = 0.38.*

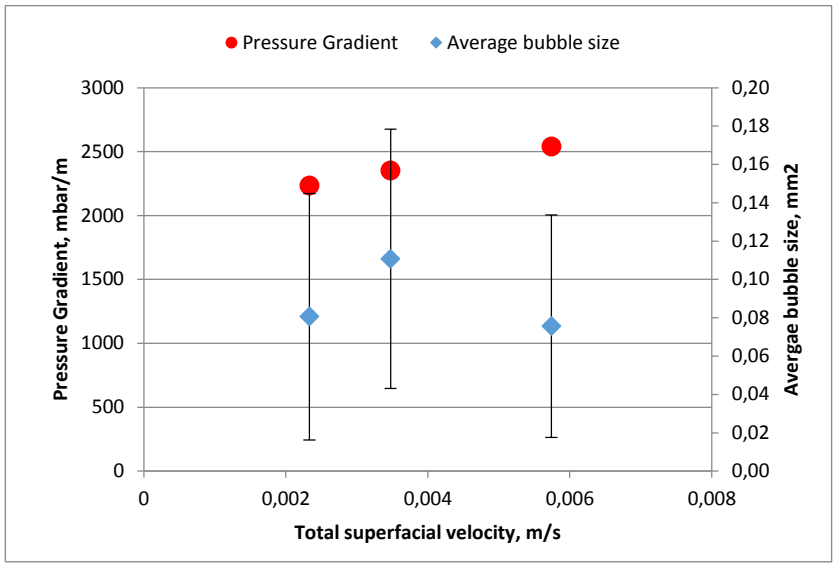

Figure 18. *Pressure gradient and average bubble size vs* u_t *at* $f_g = 0.24$

Conclusions

The following conclusions can be drawn from our experimental investigation using a model fracture:

- The increase in total superficial velocity of foam injection resulted in an increase in pressure gradient. The pressure gradient increase is not proportional to superficial velocity, but reflects shear-thinning behavior, with an average exponent of about (-0.82).
- The pressure-gradient data for in-situ generated foam reveals the existence of foam two foam-flow regimes, high- and low-quality regimes, as seen in 3D porous media.
- The high-quality regime is evidently the result of reduced and fluctuating foam generation, not due foam collapse at the limiting capillary pressure.
- For three low-foam qualities, the images at different superficial velocities show no significant change in average bubble size, but the bubbles are smaller than pores.

Acknowledgment

The authors acknowledge Saudi Aramco for providing the scholarship for Mr. AlQuaimi, and also the generous support provided by the sponsors of the Joint Industry Project on Foam for Enhanced Oil Recovery at Delft University of Technology.

References

Allan, J., & Sun, S. Q. (2003). *SPE-84590-MS. Controls on Recovery Factor in Fractured Reservoirs: Lessons Learned from 100 Fractured Fields*. Paper presented at the SPE Annual Technical Conference and Exhibition . Denver, Colorado, U.S.A. 5 – 8 October 2003.

AlQuaimi, B. I., & Rossen, W. R. (2017a). Capillary Desaturation Curve for Residual Nonwetting Phase in Natural Fractures. *Submitted to International Journal of Multiphase Flow*.

AlQuaimi, B. I., & Rossen, W. R. (2017b). Study of foam generation and propagation in fully characterized physical-model fracture. *manuscript in preparation*.

Alvarez, J. M., Rivas, H. J., & Rossen, W. R. (2001). Unified Model for Steady-State Foam Behavior at High and Low Foam Qualities. *SPE journal*. doi:10.2118/74141-PA

Buchgraber, M., Castanier, L. M., & Kovscek, A. R. (2012). *Microvisual investigation of foam flow in ideal fractures: role of fracture aperture and surface roughness.* Paper presented at the SPE Annual Technical Conference and Exhibition.

Chen, C. Y., Horne, R. N., & Fourar, M. (2004). Experimental study of liquid-gas flow structure effects on relative permeabilities in a fracture. *Water resources research, 40*(8).

Fernø, M. A., Gauteplass, J., Pancharoen, M., Haugen, Å., Graue, A., Kovscek, A. R., & Hirasaki, G. (2016). Experimental Study of Foam Generation, Sweep Efficiency, and Flow in a Fracture Network. *SPE journal, 21*(4), 1140. doi:10.2118/170840-PA

Fjelde, I., Zuta, J., & Duyilemi, O. V. (2008). *Oil Recovery from Matrix during CO2-Foam Flooding of Fractured Carbonate Oil Reservoirs.* Paper presented at the Europec/EAGE Conference and Exhibition, 9-12 June 2008, Rome, Italy.

Hakami, E., & Larsson, E. (1996). *Aperture measurements and flow experiments on a single natural fracture.* Paper presented at the International Journal of Rock Mechanics and Mining Sciences & Geomechanics Abstracts.

Haugen, Å., Mani, N., Svenningsen, S., Brattekås, B., Graue, A., Ersland, G., & Fernø, M. A. (2014). Miscible and immiscible foam injection for mobility control and EOR in fractured oil-wet carbonate rocks. *Transport in porous media, 104*(1), 109-131.

Khatib, Z., Hirasaki, G., & Falls, A. (1988). Effects of capillary pressure on coalescence and phase mobilities in foams flowing through porous media. *SPE reservoir engineering, 3*(03), 919-926.

Kovscek, A., Tretheway, D., Persoff, P., & Radke, C. (1995). Foam flow through a transparent rough-walled rock fracture. *Journal of Petroleum Science and Engineering, 13*(2), 75-86.

Prigiobbe, V., Worthen, A. J., Johnston, K. P., Huh, C., & Bryant, S. L. (2016). Transport of Nanoparticle-Stabilized CO $$_2$$ 2 -Foam in Porous Media. *Transport in porous media, 111*(1), 265-285. doi:10.1007/s11242-015-0593-7

Rabbani, A., Jamshidi, S., & Salehi, S. (2014). An automated simple algorithm for realistic pore network extraction from micro-tomography Images. *Journal of Petroleum Science and Engineering, 123*, 164-171.

Ransohoff, T., & Radke, C. (1988). Mechanisms of foam generation in glass-bead packs. *SPE reservoir engineering, 3*(02), 573-585.

Rossen , W. R., & Wang , M. W. (1999). Modeling Foams for Acid Diversion. *SPE journal, 4*(2), 92-100. doi:10.2118/56396-PA

Steinsbø, M., Brattekås, B., Ersland, G., Bø, K., Opdal, I., Tunli, R., Graue, A., & Fernø, M. (2015). *Foam as mobility control for integrated CO2-EOR in fractured carbonates.* Paper presented at the IOR 2015-18th European Symposium on Improved Oil Recovery, Dresden, Germany 14-16 April 2015.

Witherspoon, P. A., Wang, J. S., Iwai, K., & Gale, J. E. (1980). Validity of cubic law for fluid flow in a deformable rock fracture. *Water resources research, 16*(6), 1016-1024.